Analytical Methods

Accepted Manuscript

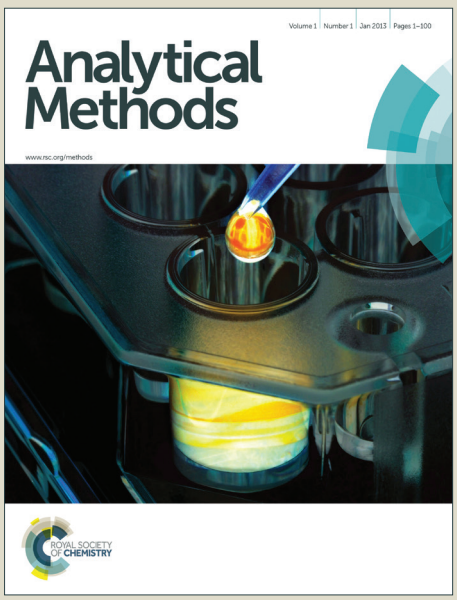

This is an *Accepted Manuscript*, which has been through the Royal Society of Chemistry peer review process and has been accepted for publication.

Accepted Manuscripts are published online shortly after acceptance, before technical editing, formatting and proof reading. Using this free service, authors can make their results available to the community, in citable form, before we publish the edited article. We will replace this *Accepted Manuscript* with the edited and formatted *Advance Article* as soon as it is available.

You can find more information about *Accepted Manuscripts* in the Information for Authors.

ROYAL SOCIETY OF CHEMISTRY

www.rsc.org/methods

Hyperspectral imaging in tandem with multivariate analysis and image processing for non-invasive detection and visualization of pork adulteration in minced beef

Mohammed Kamruzzaman[a,b*], Yoshio Makino[a*], and Seiichi Oshita[a]

[a]Graduate School of Agricultural & Life Science, The University of Tokyo, Japan.

[b]Department of Food Technology and Rural Industries, Faculty of Agricultural Engineering & Technology, Bangladesh Agricultural University, Mymensingh-2202, Bangladesh.

Abstract

Pork adulteration in minced beef was detected for the first time using a hyperspectral imaging (HIS) technique. Minced beef samples were adulterated with minced pork in the range of 2%–50% (w/w) at approximately 2% intervals. Images were acquired using a visible near-infrared hyperspectral imaging (VNIR-HSI) system and their spectral data were extracted. Several data pre-treatments and different linear multivariate analyses, namely partial least squares regression (PLSR), principal component regression (PCR), and multiple linear regression (MLR), were investigated

* *Corresponding author. E-mail: amakino@mail.ecc.u-tokyo.ac.jp, Tel:* +813 5841 5361

* *Corresponding author. E-mail: mohammed.kamruzzaman@bau.edu.bd, Tel:* +88 01849 113583

to determine the predictive ability of VNIR–HSI in detecting pork meat adulteration in minced beef. PLSR had a better performance than that of PCR for predicting pork adulteration in minced beef. Only four wavelengths centered at 430, 605, 665, and 705 nm were selected as the important wavelengths to build MLR model for visualizing the distribution of adulteration. The results confirm that HSI can be used to provide a rapid, low cost, and nondestructive testing technique for adulterate detection in minced meat.

Keywords: Hyperspectral imaging; adulteration; minced beef; minced pork; multivariate analysis.

1. Introduction

Meat is one of the most commonly consumed high value food items throughout the world. Because of its high value, there is always an opportunity for fraudulent replacement of premium quality material with lower–grade, cheaper meats.[1] Although the determination of meat authenticity and the detection of adulteration have received ample attention in the meat industry, the prevalence of meat fraud is not easy to assess.[2] Therefore, to ensure consumer health and to maintain consumers' confidence and satisfaction, it is necessary to have reliable analytical methods to confirm meat authenticity and detection of meat adulteration. Any such method should be rapid, noninvasive, accurate, and spatially located.[3] HSI techniques have shown the potential

to meet these criteria. The technology has recently emerged as a powerful technique that integrates spectroscopy and imaging to extract both spectral and spatial information from a sample. The HSI system generates images in a three-dimensional form called "hypercube" which facilitates the determination of chemical compositions of several samples in addition to visualizing chemical distribution within the same sample. Associated with multivariate data analysis, HSI techniques have proven to be powerful tools for quantitative and qualitative analyses of a wide range of materials for a large number of chemical and physicochemical properties.[4-6] In particular, this technology has already received considerable attention for assessing different quality attributes and safety parameters in meat and meat products.[7-22]

Minced beef is the major ingredient in a variety of high volume meat products such as hamburgers, patties, meatballs, sausages, and salami. It is considered superior and commands a higher price compared with other types of minced meat, such as chicken and pork, thereby making it more susceptible for potential fraud or adulteration. Therefore, developing a smart system based on HSI to detect adulteration is crucial for the meat industry. However, it is imperative to emphasize that the present HSI system is not yet ready for implementation in meat processing industries because of its high dimensionality of spectral data as well as time constraints for image acquisition and

subsequent image analyses.[5] Therefore, the challenge is to search for the most sensitive wavebands for the development of an optimized "multispectral" imaging system that could be directly implemented in industrial applications. In practice, for the design of rapid, low-cost, multispectral imaging systems, either the visible-shortwave, near-infrared region (400-1000 nm) measured by CCD array detectors, or the region between 900-1700 nm or 900 and 2500 nm, measured with InGaAs detectors, are available. The 400-1000 nm range is advantageous because of the wide availability and low cost of charge-coupled device (CCD) detectors compared with InGaAs detectors.[4] To the best of our knowledge, only one study has detailed the detection of pork adulteration in minced lamb using NIR-HSI in the spectral range of 900-1700 nm.[15] No research has yet been conducted for detecting adulteration in minced beef using HSI. Our previous work has shown the potential of using VNIR-HSI as a rapid method to detect horsemeat adulteration in minced beef.[17] The present study is a further step towards the development of a VNIR-HIS system (400-1000 nm) as a rapid and non-destructive analytical tool to detect adulteration in minced beef by pork. The specific objectives of the current study were: (1) to build PCR and PLSR models for predicting pork adulteration in minced beef; (2) to identify optimum wavelengths that could be used to develop an on-line multispectral imaging system for predicting

adulteration in minced beef; (3) to develop image-processing algorithms based on optimum wavelengths, to generate prediction maps for visualization of adulteration levels in minced beef.

2. Materials and methods

2.1 Sample preparation

Minced beef and pork were collected from a local supermarket. The minced beef samples were adulterated by mixing minced pork in the range of 2%–50% (w/w), at approximately 2% increments. The minced beef and pork were individually weighed and thoroughly mixed and homogenized to obtain a total sample weight of 32 g. A total of 25 samples (one sample per adulterate level × 25 levels) were prepared and used as a calibration set. On the other hand, a total of 13 samples were prepared in a different batch as a testing dataset in the same range at approximately 4% increments. These samples were used exclusively to validate the performance of calibration model. The minced meat was placed in a circular metal can and imaged using the HSI system.

2.2 Hyperspectral imaging system, image acquisition, and correction

A laboratory-based VNIR-HSI system in the spectral range of 400-1000 nm was used to acquire images of the tested samples in the reflectance mode. The detailed description of the system is presented elsewhere.[23] In short, the system composed of a 12-bit CCD

camera (MC1002PF, Texas Instruments, USA), a spectrograph (ImSpector, V10, Spectral Imaging Ltd., Oulu, Finland), a C-mount lens, a light source consisting of a 150-W tungsten halogen lamp (ColdSpot PCS-UHX, NPI, Tokyo, Japan) and a 150-W Xe lamp (Super Bright 152S, SAN-EI Electric, Osaka, Japan), a stage control unit (Model SGSP 26- 200, Sigma–Kaki Co., Ltd., Tokyo, Japan), and a computer supported with a data acquisition and control software system (SpectrumAnalyzer, version 1.8.5, JFE, Techno-Research Corporation, Tokyo, Japan). The entire acquisition was carried out in a dark room (temperature = 20°C and humidity = 65%) to avoid any stray light from the surrounding environment. The image acquisition procedure was operated using the computer coupled with the Spectrum Analyzer software. The exposure time of the CCD camera was set to 9.4 ms. The speed of the translation stage was 2.08 mm/s. Each image was acquired in the spectral range of 400-1000 nm with 5 nm intervals between contiguous bands, thus producing a hyperspectral image with 121 bands. However, the spectral data for further processing were limited to 117 bands (420-1000 nm) to avoid low signal- to -noise ratio.

Spectral data collected from a CCD device contained detector signal intensity and not actual reflectance values. Therefore, it is generally more useful to correct or transform the raw data into reflectance or absorbance units. The image correction was carried out

by acquiring white and dark reference images. The dark reference image (approximately 0% reflectance) was obtained by completely closing the lens of the camera with its opaque cap, while the white reference image was acquired from a uniform, stable, and high reflectance white calibration tile made of Teflon (approximately 100% reflectance). The corrected hyperspectral image (R) was then calculated by using the following equation:

$$R = \frac{R_0 - D}{W - D} \qquad (1)$$

R_0 is the raw hyperspectral image, W is the reference image, and D is the dark image. This equation transforms the reflectance value of all pixels from the raw hyperspectral image having absolute reflectance values (in arbitrary reflectance units) to relative reflectance values (unitless).

2.3 Image segmentation and extraction of spectral data

Each hyperspectral image was segmented to isolate the minced meat from the background of the sample. A binary mask image was constructed by subtracting an image of lower reflectance (425 nm) from an image of higher reflectance (875 nm) followed by a simple thresholding at a value of 0.22. Morphological operations were performed on the resultant binary mask to remove the isolated parts (if any) originating from the edges of metal cans. This step resulted in a final mask containing only minced

meat, which was then used as the main region of interest to extract spectral information from the corrected hyperspectral image. Only one average spectrum was obtained to represent each sample and the same procedure was repeated for all hyperspectral images of the tested samples. Background segmentation and extraction of spectral data from hyperspectral images were programmed in Matlab (The Mathworks Inc., Mass, USA).

2.4 Multivariate spectral analysis

After extracting the spectral data, the next stage is to establish reliable multivariate calibration models. However, it is necessary to mitigate the noise in the data (if any) to enhance the signal-to-noise ratio to obtain a good and robust prediction model. Therefore, prior to the multivariate modelling, different pre-processing routines such as multiplicative scatter correction (MSC), standard normal variate (SNV) and second derivative were separately applied to the spectral data.

Calibrations and predictions of adulteration in minced beef samples based on full spectra (117 variables) were established using two linear chemometric algorithms, namely partial least-squares regression (PLSR) and principal component regression (PCR). The calibration models were strictly built using the calibration dataset and optimized using leave-one-out cross-validation. The performances of the developed calibration models were further validated using an independent testing set. The optimum

number of latent factors (LFs) or principal components (PCs) to be included in the calibration models was selected at the lowest value of prediction error sum of squares (PRESS) that demonstrates the sum of squares of deviation between predicted and reference values for cross validation models. The predictability of the models were evaluated using the correlation coefficient in calibration (R_c), cross-validation (R_{cv}) and prediction (R_p) and the standard errors in calibration (SEC), cross-validation (SECV) and prediction (SEP).

Although HSI has a great potential in a vast number of applications, this technology suffers from several typical problems, i.e., high cost and complexity in dealing with the large volumes of data involved.[5] To solve this problem, one practical solution is band selection, which aims to use a small portion of bands to represent the whole image whilst maintaining a good performance of analysis. Removal of less informative bands is useful not only to save computational cost and storage space but also to improve the performance and accuracy of the models.[24] In this study, regression coefficients (also called β coefficients) resulting from the best model were plotted and the individual wavelength corresponding to the large values (regardless of the sign) were picked up as important wavelengths. Selected important wavelengths were then used to establish multiple linear regression (MLR) models to predict the level of adulteration in minced

beef and for spatial visualization of adulteration with the aid of multivariate image processing. All multivariate spectral data analyses were performed in Unscrambler (CAMO, version 10.3).

2.5 Multivariate image analysis

The advantage of using HSI over spectroscopy resides in applying the model obtained from the average spectra to each pixel in the image; thus, obtaining a "prediction map" composed of thousands of predicted values. This prediction map was created by applying the MLR model to each pixel in the image. At first, the spectral image at selected wavelengths was unfolded into a two-dimensional matrix. This matrix was then multiplied by the regression coefficients obtained from the MLR model. The resulting matrix was refolded to form the prediction map, which exhibits the level of adulteration within all spots in the sample. A median filter with five neighboring pixels was applied to smooth and reduce the noise in the resulting map. In the prediction map, the level of adulteration was visualized by colors, where the adulteration level is ranked according to a color bar displayed along with the map. A flowchart that explains the complete analysis of the hyperspectral data starting from image acquisition to multivariate analysis and ending with the distribution map are shown in Figure 1. All image processing steps for image visualization were carried out with a program written in

Matlab.

3. Results and discussion

3.1 Spectral features of the tested samples

Figure 2a depicts the average raw reflectance spectra of all samples in the spectral range of 420-1000 nm. The spectra of the tested samples with different adulteration levels showed similar trends throughout the whole spectral range. Despite the similarity, the studied original spectra were different in reflectance values at different adulteration levels as indicated by the distance between spectral plots. In general, objects present similar spectral patterns will indicate their similarity in chemical composition. However, different concentrations of the major chemical compositions in the tested object make the difference in reflectance values. Some information regarding chemical composition and molecular structure can be obtained from the spectra for a particular absorption feature. In the visible region, the reflectance spectra had three absorption bands around 430, 560 and 595 nm. Absorption band at 430 nm is known as Soret absorption band due to a respiratory pigment haemoglobin[25] and absorption bands at 560 and 595 nm are associated with respiratory pigments, principally deoxymyoglobin or oxymyoglobin. [26, 27] All of these pigments are responsible for red meat color.[28] In addition, two small absorption bands were observed in the NIR region at 970 and 990 nm. The band at 970

nm could be assigned to the O-H stretch second overtone in water [29, 30], while the band at 990 nm could be ascribed to the second overtone C-H stretch related to fat.[26]

To correct the scatter effect, different spectral pre-treatment techniques such as SNV, MSC and second derivative (Savitsky Golay smoothing, 9-points window, 2nd order polynomial) were applied and the resulting spectra are shown in Figure 2a (raw), 2b (MSC), 2c (SNV) and 2d (second derivative). It is apparent that all the pre-treatments effectively suppressed the scatter effect. SNV and MSC worked similarly in data preprocessing and provided equivalent results as shown in Figure 2 (b and c), and this agreed well with some previous investigations.[8, 30] As expected, several new absorption spectral bands (655, 720, and 775 nm) are apparent in the second derivative spectra as illustrated in Figure 2 (d); those were difficult to understand in the original reflectance spectra as shown in Figure 2 (a).

3.2 Spectral analysis at full wavelength range

Spectral data at full wavelength range (420-1000 nm) with 117 variables were modelled using two linear multivariate methods namely PCR and PLSR and the results were compared to determine the best calibration method. For both PCR and PLSR, prediction results with raw spectra data were compared with the spectral data after treatment with different pre-processing methods (SNV, MSC, and 2nd derivative). The performance of

the calibration models was optimized by leave-one-out cross-validation and then validated by external validation in an independent validation set.

The detailed results of PCR and PLSR are listed in Table 1, where for each model, LFs/PCs, R_c, R_{cv}, R_p, SEC, SECV and SEP are reported for raw as well as pre-treated spectral data. Although these pretreatment methods reflected some improvement in the calibration models but such improvement was not significant enough because the number of LFs/PCs were much higher than those utilized in case of raw spectra. Since these models utilized more LFs/PCs compared to raw spectra, it was believed that the good calibration performance was a result of modeling the noise that was not eliminated by the corresponding pretreatments, therefore, these models were too optimistic and the good performance was not reliable. Only the models based on raw spectra will be discussed in the following sections.

It is clear from the Table 1 that PLSR performed better and always required fewer LFs than PCR. Therefore, PLSR is more parsimonious than PCR in predicting pork adulteration in minced beef. It was not surprising because PCR estimates each PC of the spectral matrix (X) to maximize the amount of explained variance without using the response variable (y), so there is no guarantee that the calculated PCs are important with respect to the response variable for prediction, while PLSR decomposes both X and y to

calculate LFs that are really important for better prediction.[31, 32] Using the raw spectra, the level of pork adulteration in minced beef was predicted by the PLSR with R_c of 0.991, SEC of 1.955%, R_{cv} of 0.987, and SECV of 2.378%, while the level of pork adulteration in minced beef was predicted by the PCR model with R_c of 0.992, SEC of 1.862%, R_{cv} of 0.986, and SECV of 2.416%. The developed models, when applied to an independent validation set, were capable of predicting with R_p of 0.974, and SEP of 4.441% using PLSR and R_p of 0.977, and SEP of 4.366% using PCR.

The results obtained in this study are in line with those reported by previous investigations with regard to predicting pork adulteration in minced lamb[15] and horsemeat adulteration in mince beef[17] using HSI. Using NIR-HSI, Kamruzzaman et al.[15] quantified pork adulteration in minced lamb with R_{cv} of 0.995 using PLSR. On the other side, Kamruzzaman et al.[17] obtained R_p of 0.990 for horsemeat quantification in minced beef using VNIR-HSI. Many researchers successfully used spectroscopic techniques for predicting adulteration in minced meat. For instance, Meza-Márquez et al.[33] reported R_p of 0.999 for predicting adulteration in minced beef mixed with horsemeat using MIR spectroscopy and Morsy & Sun[34] reported R_{cv} of 0.954 for quantifying pork in fresh minced beef using NIR spectroscopy. Schmutzler et al.[35] successfully applied Fourier transform-NIR (FT-NIR) spectroscopy for detection of

pork adulteration in veal product. Raman spectroscopy was also used to detect offal (kidney, liver, heart and lung) adulteration in beefburgers[36] and horsemeat meat adulteration in minced beef.[37] Overall, the results obtained in this study demonstrated the ability of the HSI technique to predict the percentage of adulteration in minced beef with pork meat.

Based on model performance in terms of LFs/PCs, R_c, R_{cv}, R_p, SEC, SECV and SEP, it seems that, out of the two models tested, the PLSR model with raw spectra was the most appropriate for adulterate detection in minced meat. Thereafter, only PLSR model with raw spectra will be used to select important wavelengths.

3.4 Selection of important wavelengths

Using the full spectral range could imply the risk of overfitting; noise and nonlinearities that result in less accurate models. Therefore, for effective hyperspectral image analysis, there is a need to select some bands that carry significant information while reject those that carry redundant information. Optimum wavelengths may be equally or more efficient than full wavelengths, if the wavelengths that carry most information are selected.[38] In this study, the weighted regression coefficients resulting from the best PLSR model were used to select important wavelengths where variables having large regression coefficients (irrespective of sign) were considered (Figure 3). As a result,

five (430, 490, 605, 665, and 705 nm) wavelengths were identified. However, the wavelength at 490 nm was excluded because this wavelength did not enhance the predictability of the model when considered with other four selected wavelengths. Therefore, the remaining four wavelengths (430, 605, 665, and 705 nm) were then used as effective wavelengths to replace the full range spectra for predicting pork quantification in minced beef. The selected wavelengths can be used as a basis to design and develop multispectral imaging systems for real time applications.

3.5 Spectral analysis at effective wavelengths

Once the important wavelengths were selected, a MLR model was created using only these particular wavelengths. The MLR model had a good performance with R_c of 0.992, SEC of 1.831%, R_p of 0.985, and SEP of 4.172%. Although the variable numbers needed for prediction were substantially reduced from 117 to 4, however, the prediction ability of MLR model with only four important wavelengths was better than the original PLSR or PCR models at full wavelength range (117 wavelengths). The following quantitative function was obtained to generate prediction maps to show how the magnitude of adulteration varies from sample to sample, even from spot to spot within the same sample:

$$y=- 32.31-251.99 \times X_{430} + 732.19\times X_{605} -406.48 \times X_{665} + 222.08 \times X_{705} \qquad (2)$$

where X is the reflectance spectra with corresponding footnotes indicating the specific wavelengths, y is the predicted adulteration level.

3.6 Generation of the prediction map

In contrast to spectroscopy, HSI offers simultaneous measurements of spectral and spatial information; therefore, it can be used to know the chemical compositions, their quantity, and location in the sample. Because each pixel in the hyperspectral image has its own spectrum, the spectrum of any point in the sample can be used for calculating the concentrations of its constituents (e.g., the level of pork in minced beef). The results of this process are called prediction images, in which each constituent is displayed and mapped in a different visual appearance according to its concentration. It was performed by applying the MLR model (equation 2) to each pixel of the image. The predicted value of each pixel was then mapped with a linear color scale, where the different adulteration levels from large to small were shown in a different color from red to blue. In this map, pixels with similar spectral characteristics would have a similar predicted value of the color component, resulting in a similar scale in the generated prediction map. Figure 4 shows some examples of the prediction images produced for pork adulteration in minced beef. The level of adulteration from sample to sample and within the same sample was very appealing and easily distinguishable from the resulting

prediction images. These distributions are difficult to be observed by the naked eyes. Although detection of adulteration is a complex task, the results suggest that HSI could become a useful tool for rapid and nondestructive prediction of adulteration in minced meat. Previously, HSI was also successfully for creating such prediction maps of pork adulteration in minced lamb[15] and horsemeat adulteration in minced beef. [17]

4. Conclusions

In this study, a HSI technique employed in the visible and near infrared region was investigated for rapid detection and quantification of pork adulteration in minced beef. The results of this study demonstrate that VNIR-HSI in combination with appropriate data analysis can be reliably and accurately applied to detect and quantify the amount of adulterant added to the minced beef. The amount of adulteration in minced beef by pork was predicted using MLR model with R_p of 0.985 and SEP of 4.172% with only four important wavelengths. This model was then applied back to the image to visualize the adulteration pixel by pixel within the sample. The ability of the HSI technique to map the level of adulteration is unique, and is not available from the single point spectroscopic techniques. If properly adjusted and calibrated, HSI techniques could be implemented on a wide scale for laboratory and industrial usage.

Acknowledgements

The authors would like to acknowledge the financial support provided by The Japan Society for the Promotion of Science (NO. P13395) and a Grant-in-Aid for Scientific Research (JSPS NO.26395)

References

1. C. Alamprese, M. Casale, N. Sinelli, S. Lanteri and E. Casiraghi, *LWT - Food Science & Technology,* 2013, **53**, 225-232.
2. N. Z. Ballin, *Meat Science,* 2010, **86**, 577-587.
3. G. ElMasry, M. Kamruzzaman, D.-W. Sun and P. Allen, *Critical Reviews in Food Science & Nutrition*, 2012, **52**, 999-1023.
4. M. Kamruzzaman, Y. Makino and S. Oshita, *Analytica Chimica Acta*, 2015, **853**, 19-29.
5. H. Pu, M. Kamruzzaman and D.-W. Sun, *Trends in Food Science & Technology.,* 2015, 45, 86-104.
6. M. Kamruzzaman, S. Nakauchi and G. ElMasry, in *High throughput screening for food safety assessment: biosensor technologies, hyperspectral imaging and practical application*, ed. *A. K. Bhunia, M. S. Kim, C. R. Taitt*, Woodhead Publishing, Oxford, 2015, Online screening of meat and poultry product quality and safety using hyperspectral imaging, 425-466.

7. G. ElMasry, D.-W. Sun and P. Allen, *Food Research International.* 2011, **44**, 2624–2633.

8. Y.-Z. Feng and D.-W. Sun, *Talanta*, 2013, **109**, 74-83.

9. D. Barbin, G. ElMasry, D.-W. Sun and P. Allen, *Analytica Chimica Acta,* 2012, **719**, 30-42.

10. A. Iqbal, D.-W. Sun and P. Allen, *Journal of Food Engineering*, 2013, **117**, 42-51.

11. M. Kamruzzaman, G. ElMasry, D.-W. Sun and P. Allen, *Journal of Food Engineering*, 2011, **104**, 332-340.

12. M. Kamruzzaman, G. ElMasry, D.-W. Sun and P. Allen, *Analytica Chemica Acta*, 2012, **714**, 57-67.

13. M. Kamruzzaman, D. Barbin, G. ElMasry, D.-W. Sun and P. Allen, *Innovative Food Science & Emerging Technologies.* 2012, **16**, 316-325.

14. M. Kamruzzaman, G. ElMasry, D.-W. Sun and P. Allen, *Innovative Food Science & Emerging Technologies.* 2012, **16**, 218-226.

15. M. Kamruzzaman, D.-W. Sun, G. ElMasry and P. Allen. *Talanta,* 2013, **103**, 130-136.

16. M. Kamruzzaman, D.-W. Sun, G. ElMasry, and P. Allen, *Food Chemistry*,

2013, **141**, 389-396.

17. M. Kamruzzaman, Y. Makino, S. Oshita and S. Liu, *Food & Bioprocess Technology*. 2015, **8**, 1054-1062.

18. H. Pu, D.-W. Sun, J. Ma, D. Liu, and M. Kamruzzaman, *Journal of Food Engineering*, 2014, **143**, 44-52.

19. H. Pu, A. Xie, D.-W. Sun, M. Kamruzzaman and J. Ma, *Food & Bioprocess Technology*. 2015, 8, 1-16

20. J. Qiao, N. Wang, M. O. Ngadi, A. Gunenc, M., Monroy, C., Gariepy and S.O. Prasher, *Meat Science*, 2007, **76**, 1-8.

21. G. K. Naganathan, L. M. Grimes, J. Subbiah, C. R. Calkins, A. Samal and G. E. Meyer, *Computers & Electronics in Agriculture,* 2008, **64**, 225-233.

22. G. K. Naganathan, L. M. Grimes, J. Subbiah, C. R. Calkins, A. Samal and G. E. Meyer, *Sensing & Instrumentation for Food Quality & Safety*, 2008, **2**, 178-188

23. U. Siripatrawan, Y. Makino, Y. Kawagoe and S Oshita, *Talanta*, 2011, **85**, 276-281.

24. D. Wu, H. Shi, S. Wang, Y. He, Y. Bao and K. Liu, *Analytica Chimica Acta,* 2012, **726**, 57-66.

25. D. Cozzolino and I. Murray, *LWT - Food Science & Technology,* 2004*,* **37**, 447-452.

26. L. W. Mamani-Linares, C. Gallo and D. Alomar, *Meat Science,* 2012*,* **90**,

378-385.

27. J. Tang, C. Faustman and T. A. Hoagland, *Journal of Food Science*. 2004, **69**, C717-720.

28. S. Andrés, A. Silva, A. L. Soares-Pereira, C. Martins, A. M, Bruno-Soares and I. Murray, *Meat Science*, 2008, **78**, 217-224.

29. H. B. Ding and R. J. Xu, *Journal of Agriculture & Food Chemistry*, 2000, **48**, 2193-2198.

30. M. Blanco, J. Coello, H. Iturriaga, S. Maspoch and C. D. L. Pezuela, *Applied Spectroscopy*. 1997, **51**, 240-246.

31. R. B. Keithley, M. L. Heien and R. M. Wightman, *Trends in Analytical Chemistry*, 2009, **28**, 1127-1136.

32. B. M. Nicolaï, K. Beullens, E. Bobelyn, A. Peirs, W. Saeys, K.I. Theron and I. Lammertyn, *Postharvest Biology & Technology,* 2007, **46**, 99-118.

33. Meza-Márquez, O. G., Gallardo-Velázquez, T. & Osorio-Revilla, G.. *Meat Science*, 2010, **86**, 511-519.

34. N. Morsy and D.-W. Sun, *Meat Science*, 2013, **93**, 292-302.

35. M. Schmutzler, A. Beganovic, G. Böhler and C. W. Huc, *Food Control*, 2015, **57**, 258-267.

36. M. Zhao, G. Downey and C. P. O'donnell, *Journal of Agriculture & Food Chemistry*, 2015, **63**, 1433–1441.

37. I. H. Boyaci, H. T. Temiz, R.S. Uysal, H. M. Veliog˘lu, R. J. Yadegari and M. M. Rishkan, *Food Chemistry*, 2014, **148**, 37-41.

38. J. P. Wold, T. Jakobsen and L. Krane, *Journal of Food Science*. 1996, **61**, 74-77.

Figure captions

Figure 1. Flowchart of analyzing hyperspectral images for the detection and visualization of adulteration in minced beef.

Figure 2. Spectral features of raw and with various pre-treatment procedures in the spectral range of 420-1000 nm: (a) raw, (b) MSC, (c) SNV and (d) 2nd derivative.

Figure 3. Selection of important wavelengths using regression coefficients of PLSR model

Figure 4. Pixel wise prediction maps of adulteration at different levels. The number below each prediction map is the percentage of pork meat in minced beef.

Table 1. PLSR and PCR models at full spectral range based on raw as well as pre-treated spectral data (the best model indicated in bold).

Model	Pre-processing	LFs/PCs	R_c	R_{cv}	R_p	SEC (%)	SECV (%)	SEP (%)
PLSR	**None**	**3**	**0.991**	**0.987**	**0.974**	**1.955**	**2.378**	**4.441**
	2nd D	7	0.997	0.992	0.991	1.114	1.907	3.097
	MSC	6	0.996	0.989	0.980	1.367	2.190	3.764
	SNV	6	0.996	0.989	0.980	1.362	2.192	4.471
PCR	None	5	0.992	0.986	0.977	1.862	2.416	4.366
	2^{nd}D	8	0.995	0.989	0.990	1.454	2.227	3.170
	MSC	6	0.994	0.987	0.979	1.668	2.392	3.777
	SNV	6	0.994	0.987	0.979	1.661	2.386	4.467

LFs=Latent factors, PCs=Principal components, and SEC, SECV and SEP are the standard errors in calibration, cross-validation and prediction, respectively.

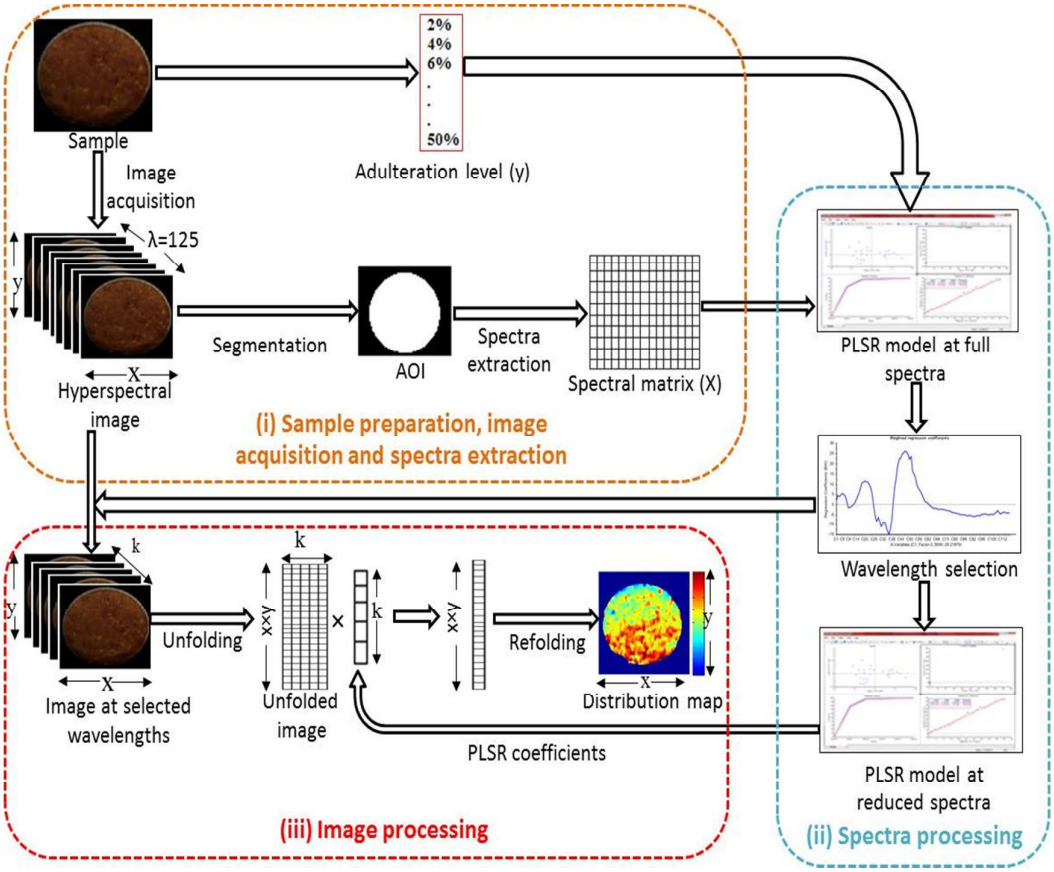

Figure 1

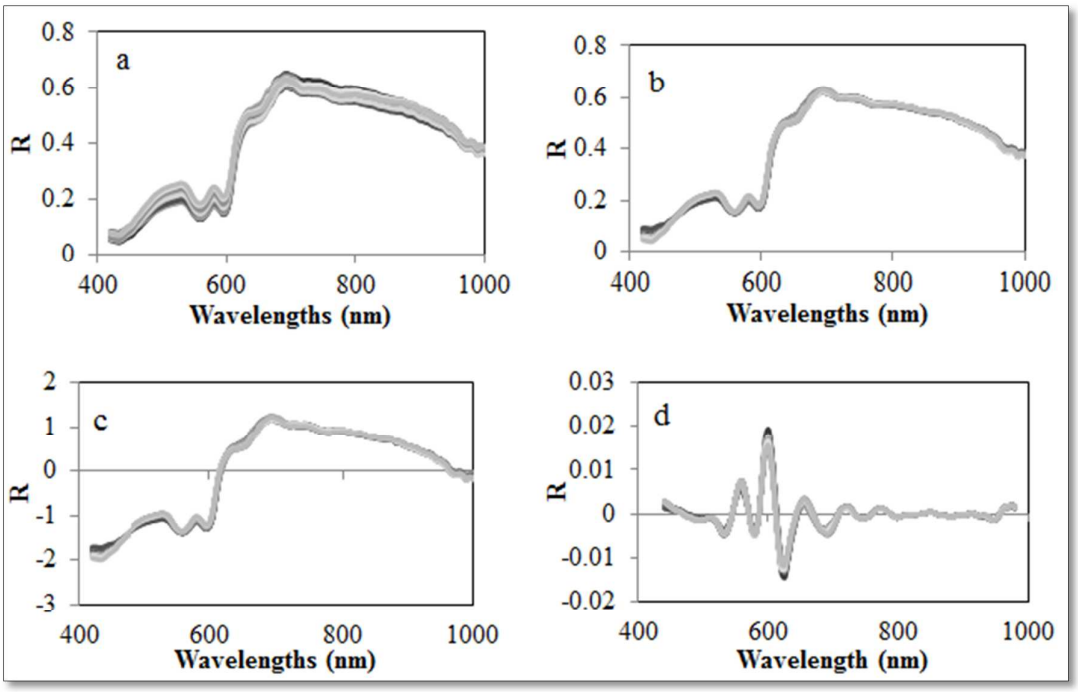

Figure 2

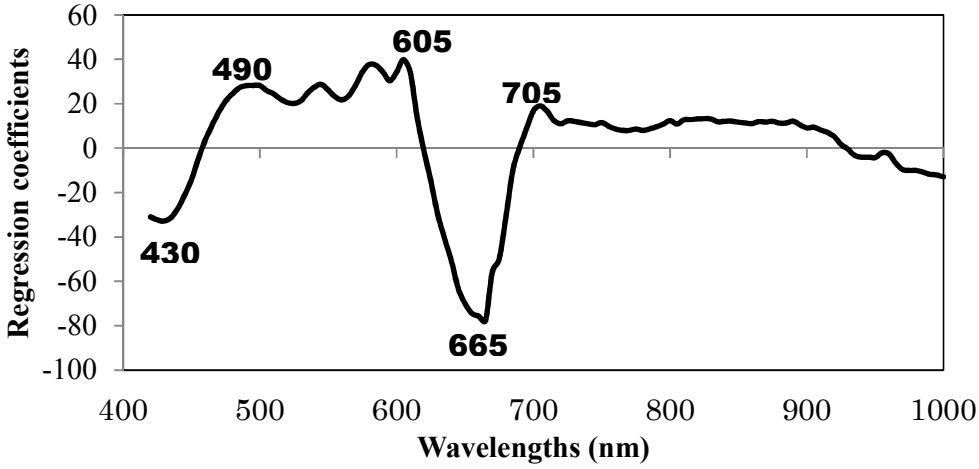

Figure 3

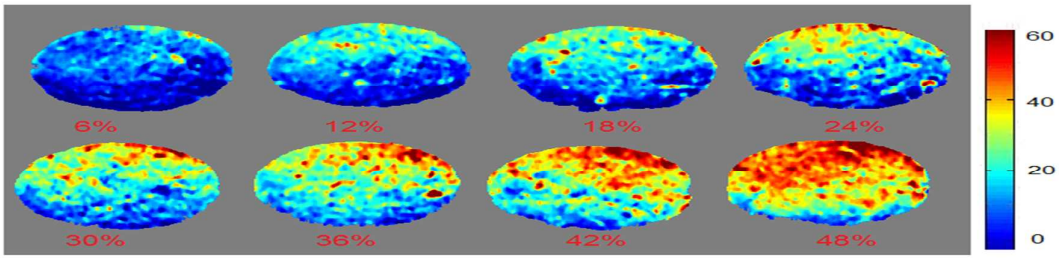

Figure 4